

Application of VOF and k-ε turbulence model in simulation of flow over a bottom aerated ramp and step structure

Talia Tokyay^{1*} and Can Kurt¹

¹Department of Civil Engineering, Middle East Technical University, Ankara, 06800, Turkey

ABSTRACT

A three-dimensional numerical model of ANSYS, Fluent (2011) was employed for studying mid to high discharge supercritical two-phase flow over a single slope spillway with a single step for aeration of the flow. In this study 18 simulations were conducted using the Volume of Fluid (VOF) method for air-water interface tracking and simple k-ε model for turbulence closure. Submerged circular shaped pipes located at the bottom of the step were utilized as aerators. Analyses concentrate on the air-entrainment phenomenon and jet-length of the flow from the step to the re-attachment point. The variables considered in the study are discharge, aerator size, different aerator arrangements, Froude number of the flow, presence of a ramp before the step and its angle. Observed jet-length values in this study were compared with two sets of empirical formulae from literature for code validation. Cross-sectional average of air concentration due to bottom aeration was determined in the streamwise direction downstream of the re-attachment of the jet. The air concentration is observed to follow a logarithmic decay in the flow direction within the de-aeration zone.

Keywords: jet-length, aerator, VOF, air-entrainment, ramp, computational fluid dynamic

INTRODUCTION

Dams have been constructed in different ways and for different purposes such as irrigation, power generation, water consumption, and flood prevention, throughout the history of civilizations. Water demand, precipitation and flow regime of the stream govern the capacity of the dams. Due to variability and instability of these factors, safety structures such as spillways are integral to dam wall structures. Since spillways are important key structures, their design life should be identical to that of the entire dam structure, and damage to spillways, such as due to cavitation, should be eliminated.

Pinto (1988) explained vaporous cavitation as the change of liquid phase to vapor phase resulting from decrease of pressure in flow due to high speeds. During this pressure decrease vapour bubbles occur and at some point these bubbles encounter higher pressure zones, where they implode. The imploding cavities in the high-pressure zones cause high pressure waves, which impact on fixed boundaries and could cause cavitation damage to the fixed boundaries. The continuous impacting of these high-pressure waves could remove small particles from the surface of structures and could lead to significant damage to the structure in time (Kells and Smith, 1991). Some of the real-life examples of cavitation damage to the structures are listed by Kramer (2004).

Estimating the cavitation potential can assist in prevention of cavitation damage to the structure. Most of the approaches in the literature for predicting cavitation potential of a flow are based on velocity of the flow. Cassidy and Elder (1984) stated that a flow with 11 m·s⁻¹ velocity can damage a concrete channel bed with irregularities. Volkart and Rutschmann (1991) stated the limit for cavitation velocity for a completely smooth concrete surface between 22 m·s⁻¹ and 26 m·s⁻¹. Oskolkov and Semenov (1979) stated a cavitation limit of operating heads exceeding 50–60 m. A more general approach

employs a cavitation number (index) which is a special form of Euler Number (Aydin, 2005) given in Eq. 1. Pinto (1988) states a cavitation risk for $\sigma < 0.25$.

$$\sigma = \frac{(P_0 - P_v)}{\rho U_0^2 / 2} \quad (1)$$

where; σ is the cavitation number, P_0 is the local pressure including atmospheric pressure, P_v is the vapor pressure, ρ is the density of the fluid and U_0 is the average flow velocity.

Cavitation damage could be mitigated by aerating the flow. Bottom aeration increases the air void ratio, which causes the water/air mixture to be more compressible. Higher compressibility lowers the pressure wave velocity and consequent impact of pressure waves. Aeration also increases the dissolved oxygen of the water and provides better dissolved oxygen values for the downstream natural life and fishery (Arantes et al., 2010). To this end, spillways designed to carry medium to high discharges, which are under a high risk of cavitation, often employ stepped structures to produce aeration zones for the flow. The aeration over the steps is often made possible by chimneys built on the side of the steps that allow air-entrainment from one side of the flow. The air-entrainment is further made possible by use of deflecting chutes, which are also known as ramps, located just before the steps. In this study flow over a ramp and step structure is simulated with a numerical model.

The flow over a ramp and step could be separated into three major zones. The first zone is the approach zone. This zone consists of the flow upstream of the step over the spillway, and it ends just before the start of the ramp as shown in Fig. 1. This region is immediately followed by a transition zone over the ramp where flow gains upward momentum. Over the step, we can observe the aeration zone, where trajected nappe flow entrains air both from the upper and the lower interface. The aeration zone ends at the location where the flow re-attaches to the spillway surface. In Fig. 1, the location of re-attachment is shown with x_r . With the re-attachment of the flow the de-aeration zone begins.

* To whom all correspondence should be addressed.
e-mail: talia.ekin.tokyay@gmail.com

Received 19 Feb 2018, accepted in revised form 4 April 2019.

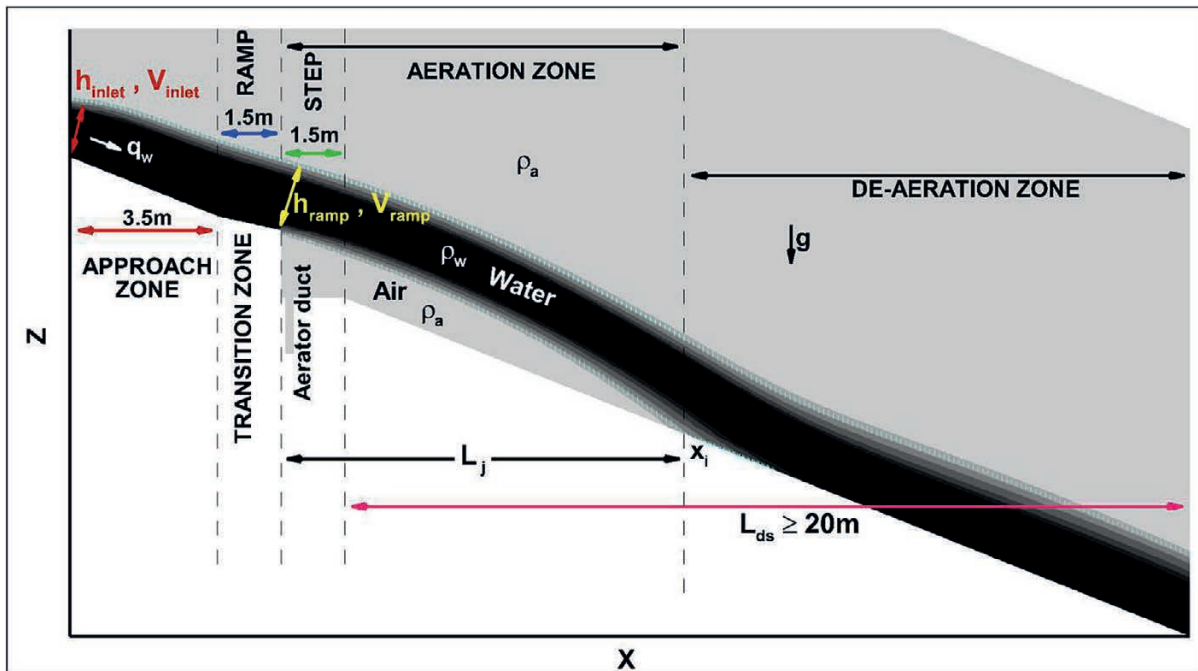


Figure 1
Sketch of the computational domain and definition of some parameters

Generally, experimental models are used for design of hydraulic structures; however, in studies where two fluids with very different properties are interacting, such as where flowing water entrains air, the scale effects become important. Most open-channel flow physical model studies are based on Froude similarity. In the case of a physical model in which air-entrainment is studied, the Weber number becomes important as it represents the surface tension effects. However, it is often difficult to achieve both Weber and Froude similarity in an experimental setting. In physical model studies it is commonly observed that larger scale models (smaller prototype/model scale ratios) give more realistic results. Due to small prototype/model scale ratios being needed for realistic results, the economy of the experiment is greatly compromised. Lee and Hoopes (1996) indicated scale effects and errors from physical model observations as one of the reasons for cavitation damage experienced in prototype spillways. Chanson (1990), who studied air demand of the Clyde Dam spillway with a 1:15 scale model, later stated that physical model studies and prototype results are far from being similar.

Air-entrainment ratio has been found to be related to some independent variables, such as slope of spillway and aerator, heights of the ramp and the offset, flow depth, Froude number and cavity sub-pressure (Rutschmann and Hager, 1990).

In literature, there are studies that employed the best of both experimental and numerical investigations of these flows. In the study of Arantes et al. (2010), experimental and computational methods were employed concomitantly. As a result, it was found that calibrated numerical models can be used for determination of bottom inlet spillway aerators.

Jet-length is a common parameter used in air-entrainment of spillway flow studies. Most of the empirical equations use jet-length for determining the air-entrainment ratio. The first study that offered such an empirical equation for jet-length is

that of Schwartz and Nutt (1963). Likewise, Pan et al. (1980) and Pinto et al. (1982) showed a relation between geometry of jet-length and air-entrainment. In the study of Kokpinar and Gogus (2002), the major forces in an open channel flow are listed as inertial, gravitational and pressure forces. In the study of Tan (1984), which is similar to the study of Rutschmann and Hager (1990), jet-length was based on sub-pressure number, P_N , which is a function of atmospheric and lower nappe cavity pressure and gravitational forces.

Different from air-entrainment ratio and jet-length studies, there are studies on aerator spacing on a spillway in order to maintain continuous aeration (Lesleighter and Chang, 1981; Pinto et al., 1982). Kells and Smith (1991) proposed limits for maximum air concentration of 45% and minimum of 8% for the proper protection of the spillway structure from cavitation.

In a recent numerical study of Aydin and Ozturk (2009), commercial CFD software was used for numerical simulation of flow over a stepped spillway with the Algebraic Slip Mixture (ASM) method and the k-ε model. The geometry of the model was based on the prototype geometry of the study of Demiroz (1985).

METHODS

The major advantage of numerical models over physical ones is their economy while eliminating scale effects. The aim of the current study is to investigate the effect of ramp angle, flow discharge, aerator size and arrangement over the jet-length, amount of air-entrainment, and general flow structure. For this purpose, a three-dimensional model is developed using ANSYS Fluent. The Volume of Fluid (VOF) method for air-water interface tracking and the simple k-ε model for turbulence closure were employed. Bottom aeration of flow was made possible by using circular cross-sectioned bottom aerator pipes. The diameter of the aerator pipe ($D_{aerator}$) and the ramp height (t), as shown in Fig. 2, were considered

as the variables in this study, together with the discharge of the flow (q_w), as given in Table 1, with the arrangement of the aerators on the step as presented in Fig. 4. The air-entrainment quantified in this study was solely due to the bottom aerators. The additional air-entrainment through free-surface of the flow was not considered separately in the results reported. The numerical results of this study were compared to the results obtained from the empirical formulae of previous studies from literature.

Computational domain, boundary conditions, and numerical method

The simulation domain is a long open-channel with bottom slope of $\theta = 16.70^\circ$. The channel has a rectangular cross section. The width of the channel is 5 m. In some of the simulations, a 1.5 m long ramp is attached to the domain just before the step in order to deflect the flow in the vertical direction. The step height is 1 m and aerators with circular cross-sections are placed

on the horizontal surface of the step. The length of the domain upstream of the step, L_{us} , is 5 m, and downstream of the step, L_{ds} , is greater than 20 m in all the simulations. A sketch of the side view of the channel floor with the step can be seen in Fig. 2.

The computational grid is composed of hexahedral elements (Fig. 3b). The grid sensitivity is tested for mesh sizes of 760 000, 1.2 million and 1.8 million for a single high-discharge value used in the simulations. The tested mesh with highest number of cells is found to resolve the location of free surface and the position of the re-attachment clearer than the meshes with a lower number of cells, even though the results were comparable for 1.2 and 1.8 million meshes. The mesh is kept denser in the region where water flow is expected. Larger cell sizes and a lower number of cells are used in the region above the flow for computational economy. The average cell size in the domain is taken as $(\Delta X, \Delta Y, \Delta Z) = (0.1, 0.05, 0.1)$ in meters. This average cell size is found to be small enough for the accuracy of the k- ϵ turbulence model (ANSYS, 2011).

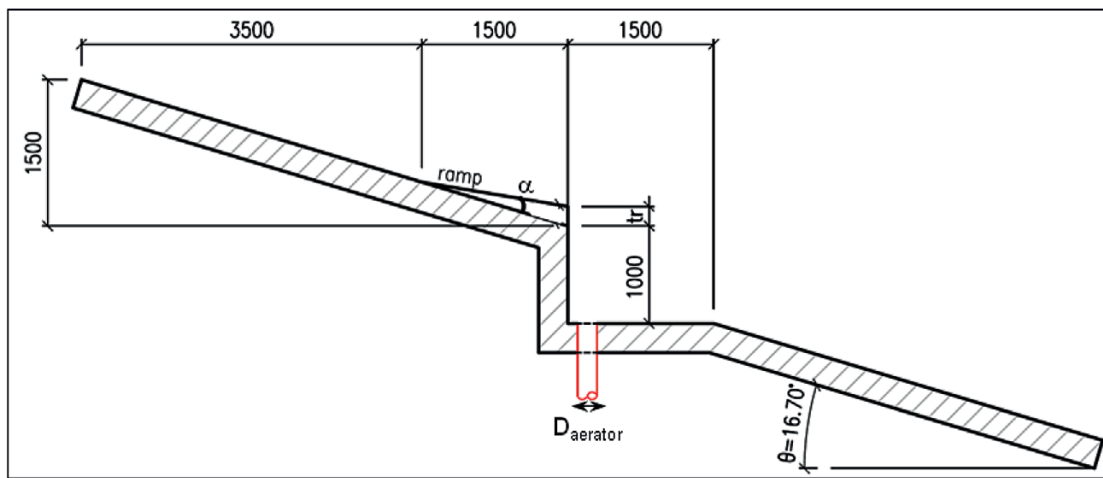


Figure 2

Side view of the channel floor with the step (dimensions in mm)

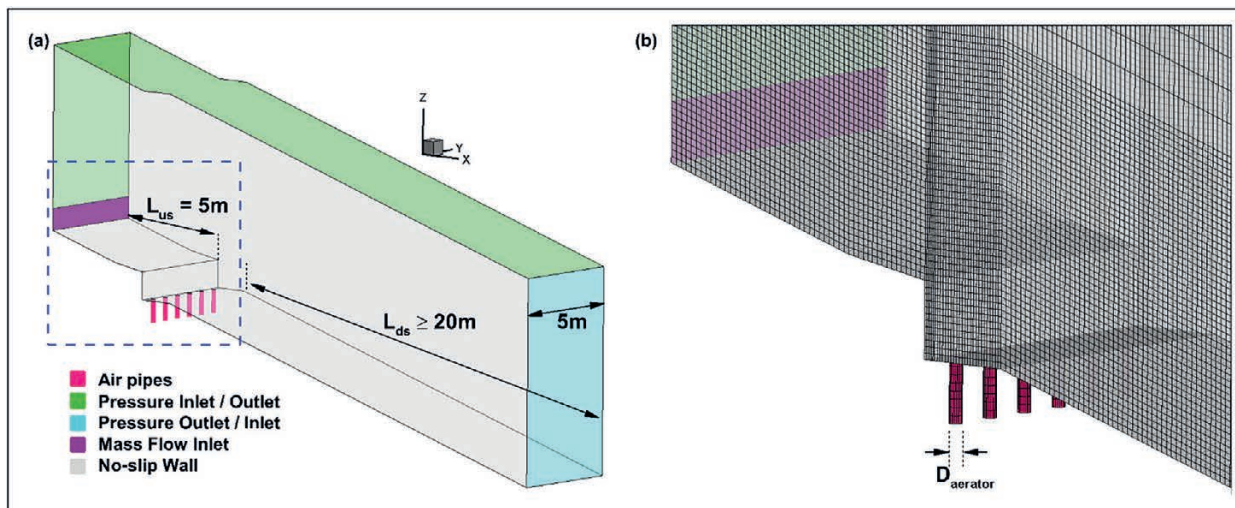


Figure 3

Simulation domain showing (a) boundary conditions and (b) computational grid. Computational grid is shown for the part of the domain isolated with dashed blue rectangle in frame (a)

The inlet is treated as a mass flow inlet as shown in Fig. 3a. The depth of the flow at the inlet is controlled by the height of the mass flow inlet boundary. The inflow depths and the respective discharges are based on the studies of Demiroz (1985) and Aydin (2005). The vertical boundary above the mass flow inlet, the top and the rightmost exit boundaries are treated as a pressure inlet/outlet. This boundary condition allows escape of air occupying the domain initially, as the inflow is introduced to the channel. The aerator pipes are taken as pressure inlets allowing entrance of air as the water flows over the step. The sides and the bottom of the domain are treated as no-slip smooth walls as shown in Fig. 3a.

In the study, the name of each case is such that first two digits show the height of the ramp in cm, the next digit is for the number of aerators that is used in the simulations, the following two digits show the unit discharge in $\text{m}^3 \cdot \text{s}^{-1} \cdot \text{m}^{-1}$, and the letter in the name is for aerator arrangement. The final digits in the name are for D_{aerator} in cm. The list of cases is given in Table 1.

The linear (L), scattered (S) and far (F) arrangement of the aerators with respect to one another are shown in Fig. 4. Some simulations have extra indicators in parentheses at the end of their names showing the inflow depths used in the simulations in order to alter the Froude number of the flow. Four different diameters of aerators are considered. These are 20, 40, 49 and 57 cm. Three different discharge values are simulated (20, 40 and $70 \text{ m}^3 \cdot \text{s}^{-1} \cdot \text{m}^{-1}$), which are identical to the ones used in the studies of Demiroz (1985) and Aydin (2005). The h_{inlet} values are also taken from these studies for the initialization of the simulations (refer to Table 1). However, in order to observe the effect of Froude number on aeration and on flow characteristics, several variations of Case 10640L40 are simulated using different h_{inlet} values. Effect of ramp height, t_r , is tested by simulating cases with no ramp (i.e., $t_r = 0$), with $t_r = 10 \text{ cm}$ ($\alpha = 3.56^\circ$), and with $t_r = 20 \text{ cm}$ ($\alpha = 7.23^\circ$). The variable α is defined as the angle that

the ramp makes with the channel floor as shown in Fig. 2. Finally, the effect of number of aerators is investigated using total of 3, 4 and 6 aerators in 3 different simulations. In these 3 simulations, total cross-sectional area of the aerators (A_a) are equal, hence aerator diameters in 2 simulations are 49 cm (Fig. 4e) and 57 cm (Fig. 4f) – which are not entirely practical; however, these were selected to keep the total aeration area identical.

In L simulations, the nearest point of the aerators is about 10 cm away from the vertical drop of the step. In S simulations, the distance between 2 rows of aerators is 10 cm for 20 cm-diameter aerators (Fig. 4c) and 40 cm for 40 cm-diameter aerators (Fig. 4d). In F simulation, one of the rows of the scattered case is further moved to the end of the step as shown in Fig. 4b. It is placed 10 cm before the downstream end of the step.

The simulated flows are turbulent, where Reynolds number ($5.5\text{--}13.5 \times 10^7$) is a function of average velocity of the approach flow, hydraulic radius and kinematic viscosity of the fluid. In this study, simplified Reynolds-Averaged Navier-Stokes (RANS) equations are solved using k- ϵ turbulence closure. The model is selected for its simplicity. Zarrati (1994) used the k- ϵ model and treated air-water mixture as a stratified flow to predict the air concentration profiles in the de-aeration zone below a spillway aerator. Bombardelli et al. (2011) applied the TruVOF method of commercial CFD software Flow3D and the k- ϵ model to study the skimming flow in a steep stepped spillway. This turbulence model is also used in 3-dimensional simulation of flow in natural river reaches (Sinha et al., 1998). Even though the k- ϵ model does not provide very detailed information on turbulence related features of the flow, it is proven to be capable of reflecting the average features of a turbulent flow adequately.

The VOF model is employed for free surface modelling by using volume fraction equations. In the simulations, water

TABLE 1
Simulation matrix

Case	t_r (cm)	Number of aerators	q_w ($\text{m}^3 \cdot \text{s}^{-1} \cdot \text{m}^{-1}$)	Aerator Arrangement	D_{aerator} (m)	h_{inlet} (m)
00620L20	0	6	20	L	0.2	0.94
00620S20	0	6	20	S	0.2	0.94
00620F20	0	6	20	F	0.2	0.94
00620L40	0	6	20	L	0.4	0.94
00620S40	0	6	20	S	0.4	0.94
10620L20	10	6	20	L	0.2	0.94
10620L40	10	6	20	L	0.4	0.94
10440L49	10	4	40	L	0.49	1.65
10340L57	10	3	40	L	0.57	1.65
10640L40(120)	10	6	40	L	0.4	1.2
10640L40(140)	10	6	40	L	0.4	1.4
10640L40	10	6	40	L	0.4	1.65
10640L40(200)	10	6	40	L	0.4	2
10640L40(250)	10	6	40	L	0.4	2.5
10670L40	10	6	70	L	0.4	2.7
20620L40	20	6	20	L	0.4	0.94

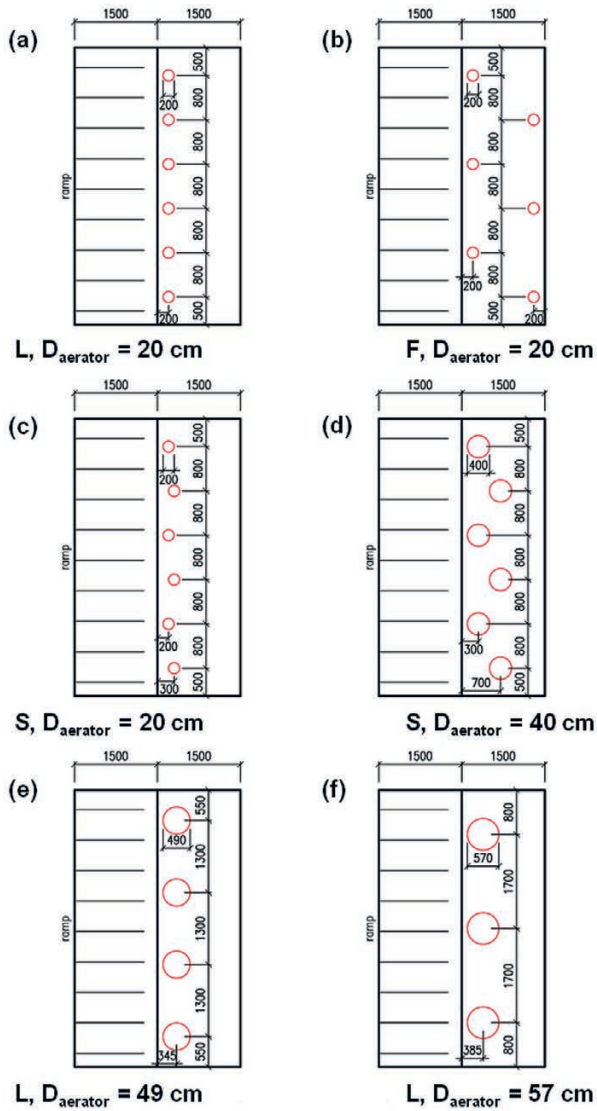


Figure 4

Aerator arrangements on the step. If not indicated otherwise, the dimensions are given in mm.

and air are selected as 2 phases that are interacting. Volume fraction of water in a cell is defined as α_w . In a cell inside the computational grid the value of α_w could be 0, if there is no water in the cell. This indicates that the cell is filled with air. If the value is equal to 1, then this shows that the cell is completely occupied by water. If $0 < \alpha_w < 1$, it indicates the presence of an interface. By solving the volume fraction of the phases with the continuity equation, tracking of the interface between the phases could be accomplished. The general equation for volume fraction is given in Eq. 2 (ANSYS, 2011).

$$\frac{1}{\rho_q} \left[\frac{\partial}{\partial t} (\alpha_q \rho_q) + \nabla \cdot (\alpha_q \rho_q \vec{v}_q) \right] = S_{\alpha_q} + \sum_{p=1}^n (\dot{m}_{pq} - \dot{m}_{qp}) \quad (2)$$

Here, \dot{m}_{qp} is the mass transfer from phase q to phase p and \dot{m}_{pq} is the mass transfer from phase p to phase q . S_{α_q} is the mass source. There is no mass transfer between phases in the simulations and an additional mass source does not exist. Due to this the right-hand side of the equation is equal to zero.

The modelling fluid for the flow is selected as water with density of $998.2 \text{ kg}\cdot\text{m}^{-3}$ and dynamic viscosity of $0.001003 \text{ Pa}\cdot\text{s}$. Initially the domain is assumed to be filled with air. In the solution methods PISO Scheme is selected as pressure-velocity coupling. PRESTO discretization for pressure and second-order upwind for volume fraction are used. First-order implicit transient formulation is used for time marching. The Courant-Friedrichs-Lewy (CFL) condition is satisfied via limiting $\text{CFL} < 1$ for the stability of the simulations.

The unsteady simulations run with a fixed time step, Δt of 0.01 s . The number of time steps is taken as 1 000. Hence, the total simulation time is 10 s. One-flow-through time is nearly 1 s for the average velocity of $20 \text{ m}\cdot\text{s}^{-1}$ and the domain length of about 20–30 m.

Table 2 lists the physical properties of the fluids used in the simulations, boundary conditions, and default coefficients of the turbulence model employed in the present study. Note that the mass flow is calculated as the product of unit discharge, domain width, and the density of water.

RESULTS AND DISCUSSION

In order to assess the amount of entrainment through the bottom aerators, an air-entrainment coefficient is used. The air-entrainment coefficient, β , can be described as $Q_{\text{air}}/Q_{\text{water}}$ where; Q_{air} is the total air flow discharge rate incoming through the aerators and Q_{water} is the water discharge rate on the spillway.

In the simulations Q_{air} is recorded at the lower boundary of the air ducts. The simulations are assumed to reach a steady

TABLE 2 Properties of the fluids, boundary conditions of the domain, coefficients of the numerical model		
Physical properties of the fluids used in the simulations		
	Density ρ ($\text{kg}\cdot\text{m}^{-3}$)	Viscosity μ (Pa·s)
Water – $\alpha_w = 1$	998.2	0.001003
Air – $\alpha_w = 0$	1.225	1.7894×10^{-5}
Boundary conditions		
	Unit discharge ($\text{m}^3\cdot\text{s}^{-1}\cdot\text{m}^{-1}$)	Mass flow ($\text{kg}\cdot\text{s}^{-1}$)
Mass flow inlet ($\alpha_w = 1$)	20–70	99 820–349 370
Pressure (kPa)		
Pressure outlet/inlet	101.3 (atmospheric)	
Pressure inlet/outlet	101.3 (atmospheric)	
Entrance boundary of air pipes ($\alpha_w = 0$)	101.3 (atmospheric)	
Velocity ($\text{m}\cdot\text{s}^{-1}$)		
Side walls of the channel, channel floor, side walls of aeration ducts	0 (no-slip condition)	
k- ϵ model constants		
$C_{\epsilon} = 1.44$		
$C_{\mu} = 0.09$		
$\sigma_k = 1.0$		
$C_{2\epsilon} = 1.92$		
$\sigma_{\epsilon} = 1.3$		

state when the Q_{air} reading of each simulation reaches a constant value. All the simulations are observed to reach steady-state after 7 s into the simulation, as shown in Fig. 5. Hence, total simulation time of 10 s produces converged steady results. Air flow discharge rates, stabilised after 7 s, represent the rate at which air is introduced into the water flow from the ducts (Fig. 5). The initial oscillation in air flow, which is observed in all the simulations, is due to the fact that all the simulations start with a domain full of air and part of the air escapes through aerators and the outflow boundary as the water enters the domain through the inlet. Based on the final Q_{air} values at the end of the simulation time, β of each flow is calculated.

The value of β signifies the air/water ratio within the flow downstream of the aerators. However, β does not represent how the air is dispersed within the flow. The air content within the flow and its cell-by-cell distribution is presented using α_w , which is obtained via Eq. 2.

Jet-length and comparison with literature

The effect of the ramp is evaluated in the simulations by using 2 different ramp heights at the approach of the step. Figure 6 shows the effect of ramp in comparison to a no-ramp case. Both simulations have identical inflow discharge and same number/

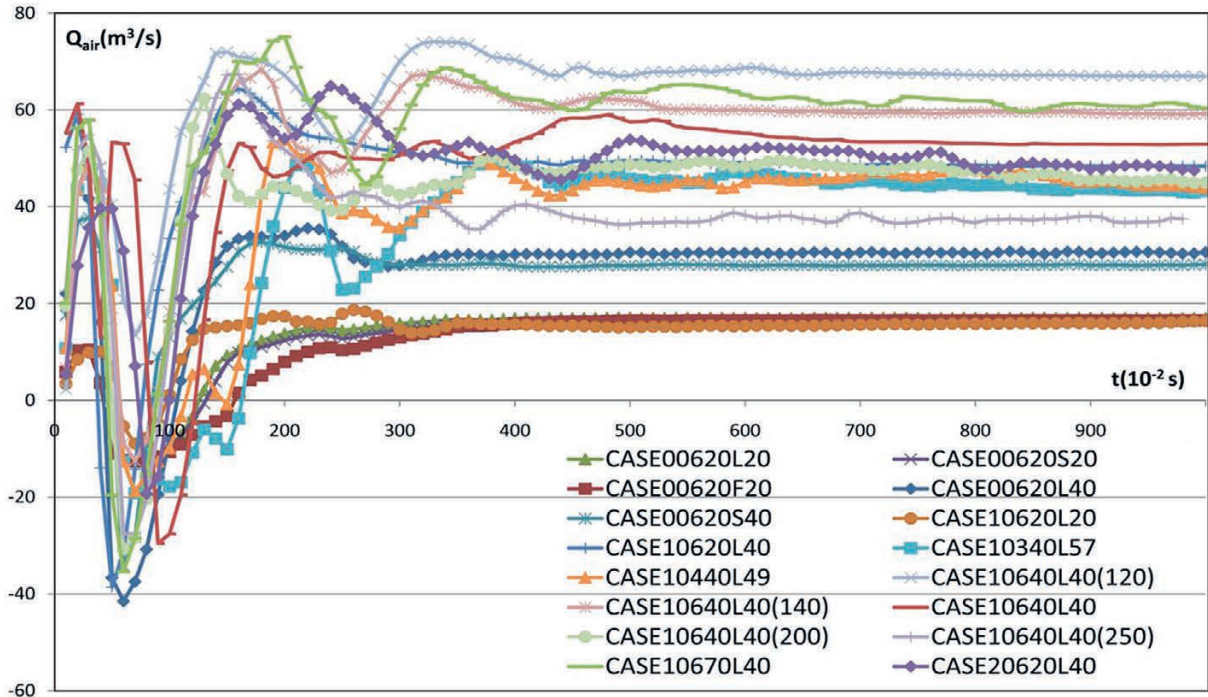


Figure 5
Temporal change in total air discharge (Q_{air}) through aeration ducts

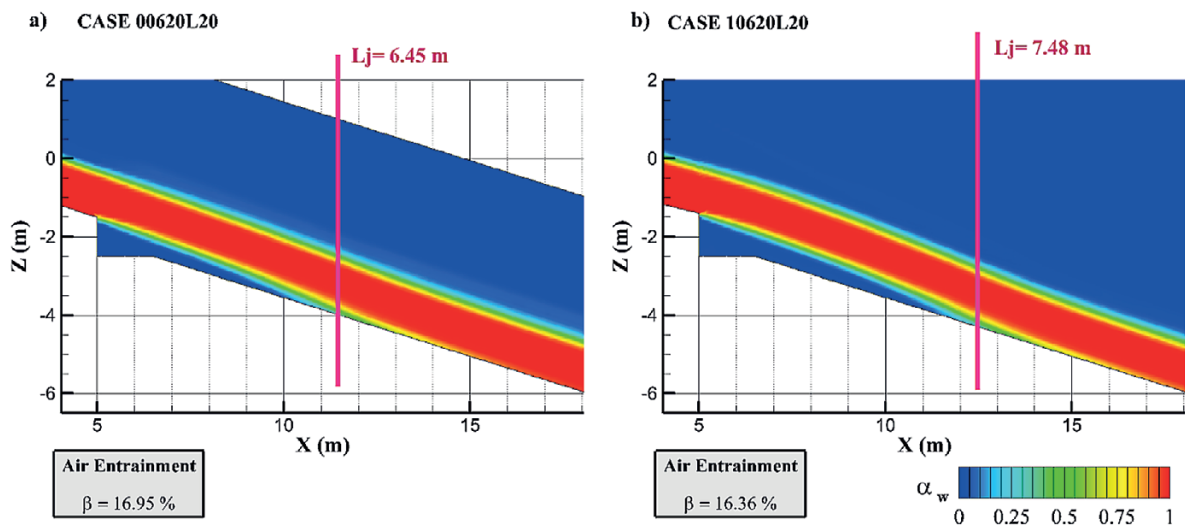


Figure 6
The water phase and jet-length (L_j) visualization for (a) Case 00620L20 (without ramp) and (b) Case 10620L20 (with 10 cm-high ramp)

size of air ducts. However, Case 10620L20 has a 10 cm-high ramp at the approach of the step (Fig. 6b) as opposed to lack of a ramp in Case 00620L20 (Fig. 6a). The ramp shows its effect in the upper air-water interface. The jet lifts off higher in the presence of a ramp as expected and this also affects the length of the jet which increases by almost a meter with the help of a 10 cm-high ramp. The jet-length, L_j , is defined as the distance between the upstream end of the step and location of re-attachment, x_r , as shown in Fig. 1. The α_w value of 0.5 is used in determination of the location of re-attachment. The 10 cm-high ramp is observed to have no significant effect on the air-entrainment coefficient, β of the flow, in the case of inflow discharge of $20 \text{ m}^3 \cdot \text{s}^{-1} \cdot \text{m}^{-1}$.

However, the higher the ramp height, the greater the change observed in the jet-length and the air-entrainment. The air-entrainment, β , increases from 30.6% to 47.6% when the ramp height increases from 0 to 20 cm for the simulations with $20 \text{ m}^3 \cdot \text{s}^{-1} \cdot \text{m}^{-1}$ inflow and six 40-cm diameter air ducts. The length of the jet increases about 4 m with the 20 cm-high ramp, which can be seen in Fig. 7. The trajectory of the jet also changes quite dramatically allowing a much larger volume of the aeration zone over the step under the jet as seen in Fig. 7b. Depth of the flow downstream of the re-attachment at $x = 20 \text{ m}$ is about 1.49 m for the case with no ramp, while with the ramp the depth increases to 1.83 m. This is basically due to the entrained air, which increases the total volume (water and air mixture) of the flow.

Identical inflow discharge with various Froude numbers is possible, if one changes the average velocity (V_{inlet}) and flow depth (h_{inlet}) at the inflow boundary (Fig. 1). The Froude number, Fr , is calculated as the ratio between the inertia and the gravitational forces as given in Eq. 3.

$$Fr = \frac{V_{\text{ramp}}}{\sqrt{gh_{\text{ramp}}}} \quad (3)$$

In this equation, g represents the gravitational acceleration, V_{ramp} represents the average cross-sectional velocity of the flow at the downstream end of the ramp, and h_{ramp} represents the depth of the flow at the downstream end of the ramp as shown in Fig. 1. In the absence of a ramp, V_{ramp} and h_{ramp} values are

simply taken at a cross section right before the vertical drop of the step.

In the current study, all the simulations conducted are in the supercritical range; however, the ones that are discussed so far have a narrow range of Froude numbers between 5.04 and 6.03. Next, we present 5 simulations that have a constant inflow discharge of $40 \text{ m}^3 \cdot \text{s}^{-1} \cdot \text{m}^{-1}$; adding on to the previous cases, these simulations have a Froude number range of 3.23–9.72. The highest flow velocity and hence the lowest flow depth at the inflow section is observed for $Fr = 9.72$. The highest Froude number case has average flow velocity of $33.33 \text{ m} \cdot \text{s}^{-1}$ and the depth of the flow is 1.2 m at the inlet. When $Fr = 3.23$, the average flow velocity and the flow depth at the inlet is $16 \text{ m} \cdot \text{s}^{-1}$ and 2.5 m, respectively.

L_j is observed to increase quite significantly as Fr increases (Fig. 8). Even though in all the simulations a ramp with height of 10 cm is used, the ramp is not observed to change the trajectory of the flow significantly in high Froude number simulations. In the high Froude number cases the inertia force dominates the flow. Therefore, the effect of gravitational force is far less significant in high Froude cases; this results in almost-straight water-air interfaces at the top of the jet parallel to the channel floor. In smaller Froude number cases the effect of the ramp becomes noticeable at the top interface.

The smallest L_j observed is about 11.2 m for the lowest Froude number case. The largest L_j is about twice as large, at around 24.5 m, compared to the lowest Froude number case. This jet-length is observed when the depth of the inflow is almost half the one in the lowest Froude number simulation.

The relation between Froude number and jet-length is shown in Fig. 9. The jet-length increases with increasing Froude number. Following the empirical relation proposed by Kokpinar and Gogus (2002), the best-fit in Fig. 9 is selected as a function of $Fr^{1.75}$. The aeration index β is calculated as 33.45% at the highest Froude number simulation, while it drops down to 18.59% at the lowest Froude number simulation. Similar to our numerical results, Terrier (2016), who studied hydraulic performance of stepped spillway aerators with a physical model, recently observed that approach flow Froude number increases the spread of the jet and value of β .

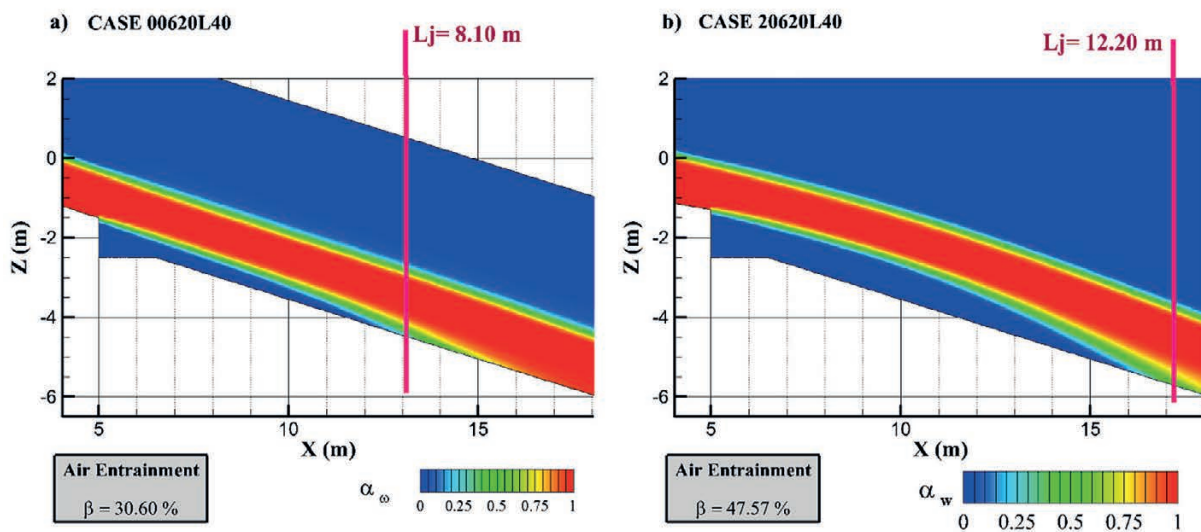


Figure 7

The water phase and jet-length (L_j) visualization for (a) Case 00620L40 (without ramp) and (b) Case 20620L40 (with 20 cm-high ramp)

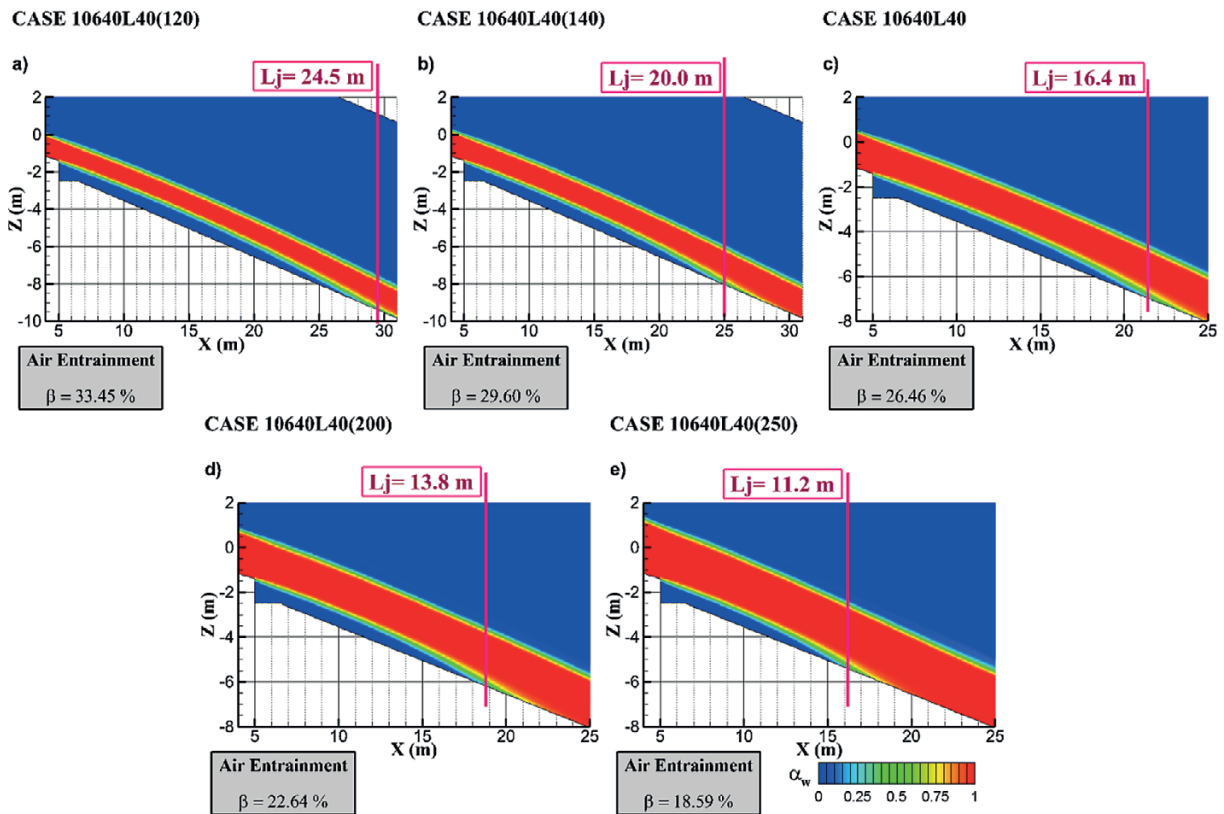


Figure 8

The water phase and jet-length (L_j) visualization of 10640L40 cases for (a) $Fr = 9.72$ ($h_{inlet} = 1.2$ m), (b) $Fr = 7.71$ ($h_{inlet} = 1.4$ m), (c) $Fr = 6.03$ ($h_{inlet} = 1.65$ m), (d) $Fr = 4.52$ ($h_{inlet} = 2.0$ m), and (e) $Fr = 3.23$ ($h_{inlet} = 2.5$ m)

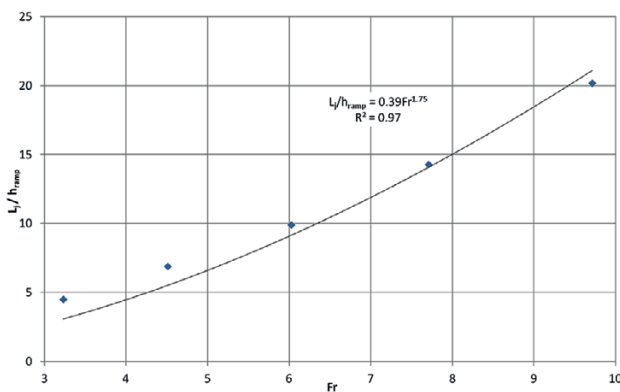


Figure 9

Change in jet-length (L_j) with respect to Froude number (Fr) of the flow upstream of the step for 10640L40 cases with $3.23 \leq Fr \leq 9.72$.

A summary of the findings of all 18 cases are given in Table 3. In the table A_a is the total area of air ducts and A_w is the area of the flow calculated with h_{ramp} . Jet-lengths (L_j) are given in 3 columns, first jet-length is the length observed in the simulations based on the position of the re-attached jet, the other two columns are for comparison with previous studies of Tan (1984) and Kokpinar and Gogus (2002), for validation purposes. The table also includes values for jet flight time, t_j , (time between flow leaving the ramp and the re-attachment). The values of t_j are presented for the current

study and that of Tan (1984). Further, the dimensionless constant K ; which represents the relation between air-entrainment and jet-length, is given in Table 3 for each simulation of the present study.

The experimental study of Kokpinar and Gogus (2002) mainly focused on the jet flows over the spillway aerators. The aim of their study was to analyse the effect of geometric properties and flow conditions on jet-length and air-entrainment capacity. Based on their experimental study and the results of the study of Demiroz (1985), some empirical formulas were developed by Kokpinar and Gogus (2002), including Eq. 4 below.

$$\frac{L_j}{h_{ramp}} = 0.28(1 + \alpha)^{0.22} Fr^{1.75} \left(\frac{t_r + H_s}{h_{ramp}} \right)^{0.44} \left[(1 + \tan\theta) \frac{A_a}{A_w} \right]^{-0.087} \quad (4)$$

The limits of Eq. 4 are $5.56 \leq Fr \leq 10.0$, $0.198 \leq (t_r + H_s)/h_{ramp} \leq 1.985$, $0 \leq \alpha \leq 9.45^\circ$, $0 \leq \tan \theta \leq 1.25$, $0.0684 \leq A_a/A_w \leq 1$, where A_a is total aeration area, A_w is area of flow over ramp, h_{ramp} is depth of flow over ramp, and H_s is the step height measured perpendicular to the inclined channel bed (Fig. 1). Many of the cases considered in the present study are within these limits. The relative flow area of air to the flow area of water is given by ratio of A_a/A_w . Both A_a and A_w are related to the geometry of the domain considered in the numerical simulations. A_a is simply calculated as the total area of pipe openings that deliver air. Similarly, A_w is related to the depth of the flow at the downstream end of the ramp and the width of the channel.

Case	h_{ramp} (m)	V_{ramp} ($m \cdot s^{-1}$)	A_a/A_w	Fr	Kokpinar and Gogus (2002)	Tan (1984)		Present study			
					L_j (m)	L_j (m)	t_j (s)	t_j (s)	L_j (m)	β	K
00620L20	1.10	18.2	0.03	5.53	5.00	5.61	0.30	0.35	6.45	16.95	0.029
00620S20	1.10	18.2	0.03	5.53	5.00	5.70	0.31	0.38	6.96	16.35	0.026
00620F20	1.10	18.2	0.03	5.53	5.00	5.65	0.30	0.37	6.65	16.50	0.027
00620L40	1.10	18.2	0.14	5.53	4.43	5.81	0.31	0.45	8.10	30.60	0.042
00620S40	1.10	18.2	0.14	5.53	4.43	5.76	0.31	0.40	7.27	27.99	0.042
10620L20	1.10	18.2	0.03	5.53	7.53	9.42	0.50	0.41	7.48	16.36	0.024
10620L40	1.10	18.2	0.14	5.53	6.68	9.43	0.50	0.56	10.10	48.37	0.053
10440L49	1.65	24.2	0.09	6.03	11.78	13.90	0.56	0.85	20.50	22.00	0.018
10340L57	1.65	24.2	0.09	6.03	11.78	13.90	0.56	0.89	21.55	21.60	0.017
10640L40(120)	1.20	33.3	0.13	9.72	22.12	22.00	0.64	0.73	24.20	33.45	0.017
10640L40(140)	1.40	28.6	0.11	7.71	16.31	17.58	0.60	0.70	20.00	29.60	0.021
10640L40	1.65	24.2	0.09	6.03	11.78	13.92	0.56	0.67	16.35	26.46	0.027
10640L40(200)	2.00	20.0	0.08	4.52	8.05	10.68	0.52	0.69	13.80	22.64	0.033
10640L40(250)	2.50	16.0	0.06	3.23	5.18	8.02	0.48	0.70	11.20	18.60	0.042
10670L40	2.70	25.9	0.06	5.04	11.84	15.19	0.57	0.69	17.90	17.25	0.026
20620L40	1.10	18.2	0.14	5.53	8.11	13.04	0.69	0.67	12.18	47.57	0.043
20620L20	1.10	18.2	0.03	5.53	9.15	13.30	0.70	0.56	10.10	20.50	0.043
00640L40	1.65	24.2	0.09	6.03	7.82	7.94	0.32	0.36	8.68	8.98	0.017

Therefore, the ratio of A_a/A_w differs from β . The β value includes the discharge rates of air and water.

Using the geometry of the simulation domain and simulation data from the present study (h_{ramp} and Fr), jet-lengths are calculated for each case based on Eq. 4. This equation does not account for the location of the aerators. Therefore, Eq. 4 predicts identical jet-lengths for cases where aerator arrangement is the only variant. Jet-lengths obtained via Eq. 4 were plotted against findings of the numerical simulations in Fig. 10. The dashed line shows a theoretical perfect agreement between numerical and experimental findings. The linear regression fit (with $R^2 = 0.76$) indicates that the physical model results are a regression factor of 1/1.4 times smaller than the numerical results.

Recording the re-attachment point in physical model studies could be difficult due to accumulation of stagnant/circulating water upstream of the re-attachment point, x_i . In the present numerical study, the re-attachment point is defined with a fixed value of $\alpha_w = 0.5$, as stated earlier. This difference in recording of the re-attachment point in physical models and numerical simulations could be the main reason for the need of a regression factor. Furthermore, the scale effects could also play a role in the difference.

Tan's (1984) study is selected for further validation of numerical results. Analytical recommendations of the study are based on geometric properties and a pressure term P_N , which is the cavity sub-pressure number. P_N is based on the pressure difference between atmospheric air pressure and lower nappe

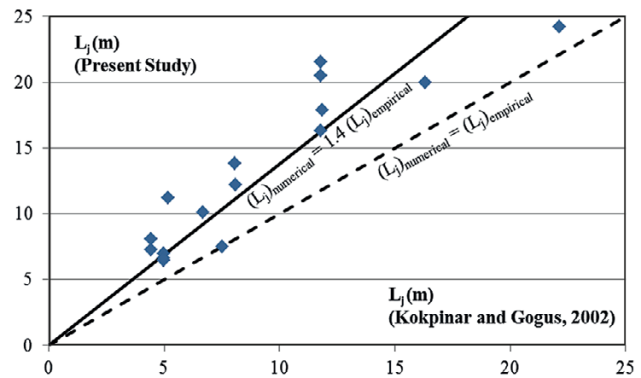


Figure 10
Jet-lengths of present numerical study versus jet-lengths calculated based on empirical formula of Kokpinar and Gogus (2002)

air pressure, ΔP , density of water ρ_w , gravitational acceleration g , and depth of the flow at the downstream end of the ramp, h_{ramp} . In the present study, the lower nappe air pressure value is obtained by reading pressure values using 100 numerical probes near the jet re-attachment. These values are averaged to obtain the cavity sub-pressure number. Inclusion of cavity sub-pressure number in the calculation of jet-length somehow accounts for the location of the aerators, hence jet-lengths calculated using Tan's expression have varying values as the cavity sub-pressure

number changes with the aerator arrangement. Equations related to the study of Tan (1984) are given in Eqs 5, 6, 7 and 8. Equations 5 and 6 are for determining the jet flight time for step/ramp aerators and only step aerators, respectively. The jet-length based on Eq. 8 is plotted against the current findings from the simulations in Fig. 11. Tan's formulation, based on pressure, estimates jet-length values closer to the present numerical results. Thus, the linear regression fit has $R^2 = 0.86$ and empirical results are a regression factor of 1/1.2 times smaller than the numerical results.

$$t_j = \frac{V_{ramp} \sin \alpha}{g(\cos \theta + P_N)} \left[1 + \sqrt{1 + 2(t_r + H_s) \frac{g(\cos \theta + P_N)}{(V_{ramp} \sin \alpha)^2}} \right] \quad (5)$$

$$t_j = \sqrt{\frac{2H_s}{g(\cos \theta + P_N)}} \quad (6)$$

$$P_N = \frac{\Delta P}{\rho_w g h_{ramp}} \quad (7)$$

$$L_j = \frac{g \sin \theta}{2} t_j^2 + V_{ramp} (\cos \alpha) t_j \quad (8)$$

The K values of the simulations are calculated using two common equations in literature. The first is given as Eq. 9 where q_a is the air-entrainment per unit chute width. Equation 10 is derived by substituting flow velocity with flow discharge, i.e., where $q_w = V_{ramp} h_{ramp}$ in Eq. 9. Table 4 shows present and previous values of K . The values of K for the present study are well within the range of the K values in the cited literature.

$$q_a = K V_{ramp} L_j \quad (9)$$

$$\beta = K \frac{L_j}{h_{ramp}} \quad (10)$$

Air concentration

In the present numerical study, the effect of the relative position of air ducts are also evaluated and observed to form an interesting phenomenon that we referred to as 'merging plumes' of aerated water'. The aim of the aerators is to create uniformly

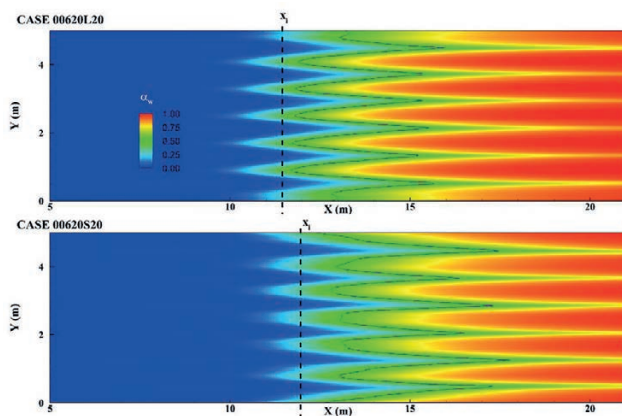


Figure 12

The mixed air-water phase distribution over the span of the spillway 5 cm above the channel bottom for Cases 00620L20 and 00620S20. Solid grey contour line shows $\alpha_w = 0.5$. Dashed lines indicate the jet re-attachment location, x_r .

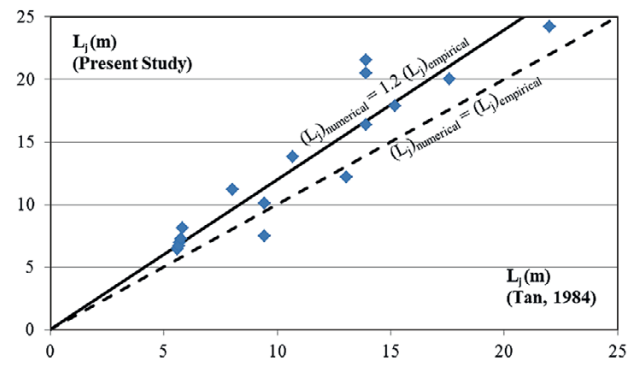


Figure 11

Jet-lengths of present numerical study versus jet-lengths calculated based on empirical formula of Tan (1984)

aerated flow over the width of the chute near the channel floor. Uniform aeration should be achieved in as short as possible x -distance downstream of the aerators with as high as possible α_w values. The air is often entrained into the water stream as the flow passes over the step in the forms of aerated plumes. This is simply due to the aerator duct arrangement. The merging of aerated plumes appears in the scattered (S) arrangement of aerators (Fig. 4).

A plane parallel to the channel floor is shown in Figs 12 and 13. The plane is 5 cm above the bottom. On this plane the aerated flow is visualized using α_w values. Figure 12 shows the aerated flow near the channel floor for simulations with unit inflow

Study	K
Pinto et al. (1982)	0.023
Wei and DeFazio (1982)	0.01~0.035
Coleman et al. (1983)	0.02
Pinto and Neidert (1983)	0.01~0.08
Hamilton (1984)	0.01~0.05
Present study	0.0165~0.0527

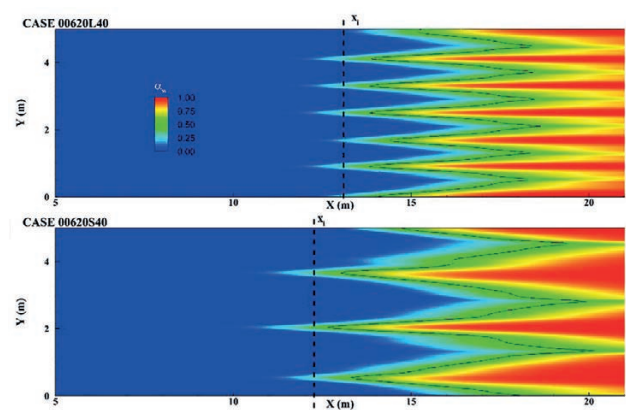


Figure 13

The mixed air-water phase distribution over the span of the spillway 5 cm above the channel bottom for Case 00620L40 and Case 00620S40. Solid grey contour line shows $\alpha_w = 0.5$. Dashed lines indicate the jet re-attachment location, x_r .

discharge of $20 \text{ m}^3 \cdot \text{s}^{-1} \cdot \text{m}^{-1}$ aerated using 20 cm-diameter aerators on the step. In both L20 and S20 cases, over the span one can observe formation of aerated plumes, where $\alpha_w < 0.5$. In case of S20, both the width and the length of these aerated plumes are observed to be longer than the ones observed in L20 case.

Figure 13 shows the aerated flow near the channel floor for simulations with unit inflow discharge of $20 \text{ m}^3 \cdot \text{s}^{-1} \cdot \text{m}^{-1}$ aerated using 40 cm-diameter aerators on the step. In the L40 case presented in Fig. 13, one can still observe the formation of 6 well-defined aerated plumes ($\alpha_w < 0.5$) near the channel floor. In the case of S40 however, only 3 separate aerated plumes are visible. This shows how 2 neighbouring air ducts work as one big air duct and in a sense decrease the total number of air ducts used in the simulation in S40.

Using the data presented in Figs 12 and 13, α_w values across the width of the chute are plotted 5 m downstream of the re-attachment point in Fig. 14. The average α_w values over the span for each case are indicated using dashed lines. The lower the α_w value, the higher the air content of the flow is. Due to the arrangement and circular cross section of aerators, a continuously homogeneous aerated region 5 cm above the channel floor 5 m downstream of the re-attachment point is not observed in any of the cases considered in the present study. The α_w values as shown in Fig. 14 follow an undulated pattern over the width of the chute. It is observed that average aeration over the span is higher via S-type aerator arrangement. The regions where α_w is less than 0.90 are assumed to be aerated as the cells in these regions have at least 10% air content in the flow. Total length of at least 10% aerated regions in Case 00620L40, 5 m downstream of x_i , is 3.74 m, while the total length of such regions is 4.28 m in Case 00620S40. It should be noted that the total width of the spillway is 5 m. Similarly, the lengths of aerated regions over the span of the spillway are 3.15 m for Case 00620L20, and 4.96 m for Case 00620S20.

Even though the size of the aerated regions is larger in S simulations, one can observe that the β values slightly decrease in these cases compared to the L arrangement of the aerators (Table 3). A similar reduction in air-entrainment is also noted in simulations 10440L49 and 10340L57 when β values are compared to the one obtained from Case 10640L40. All 3

simulations have identical total area for aeration, A_a . However, in Case 10440L49, 4 air ducts are used instead of 6 and in Case 10340L57, only 3 air ducts are used for aeration. In all 3 cases the unit water discharge is $40 \text{ m}^3 \cdot \text{s}^{-1} \cdot \text{m}^{-1}$. As given in Table 3, the value of β is around 22% for cases with fewer aerators, compared to 26% in Case 10640L40. This might be due to a reduction in suctioning effect of flow over larger diameter aerators compared to smaller diameter ones. In the S simulations, merging of air plumes creates a similar effect and in return causes reduction in values of β compared to the L simulations.

The β index is based on the amount of total air discharge entrained from the aerators. However, after the re-attachment of jet at x_p , the de-aeration zone begins as shown in Fig. 1. In this zone, the air content of the flow starts decreasing as one goes away from the re-attachment point towards the exit boundary. Based on the amount of loss of the air content, better estimation of location of the next ramp/step and aerators is possible. The cross-sectional average of air concentration (C_{air}) below the free surface of the flow is calculated over many x -planes in the streamwise direction in the de-aeration zone. The interface between the air and water at the free surface is omitted in the calculations as the results concentrate on air-entrainment through the air ducts over the step in the lower nappe. The C_{air} depends on the cross-sectional average of α_w values as given in Eq. 11. In this equation, A is the total area of the flow below the free surface.

$$C_{air} = 1 - \left(\int \alpha_w dA \right) / A \quad (11)$$

The decrease in concentration in the x -direction after x_i in the de-aeration zone could be expressed with a logarithmic decay as shown in Fig. 15 for Cases 00620L20, S20 and F20. These cases have the unit inflow discharge of $20 \text{ m}^3 \cdot \text{s}^{-1} \cdot \text{m}^{-1}$, the flow aeration is via six 20 cm-diameter aerators, and no ramp is used in the flow domain. In Fig. 15, $x - x_i$ shows the distance from the re-attachment point. In these simulations, aerator arrangement is not observed to vary the average air concentration over the streamwise direction significantly.

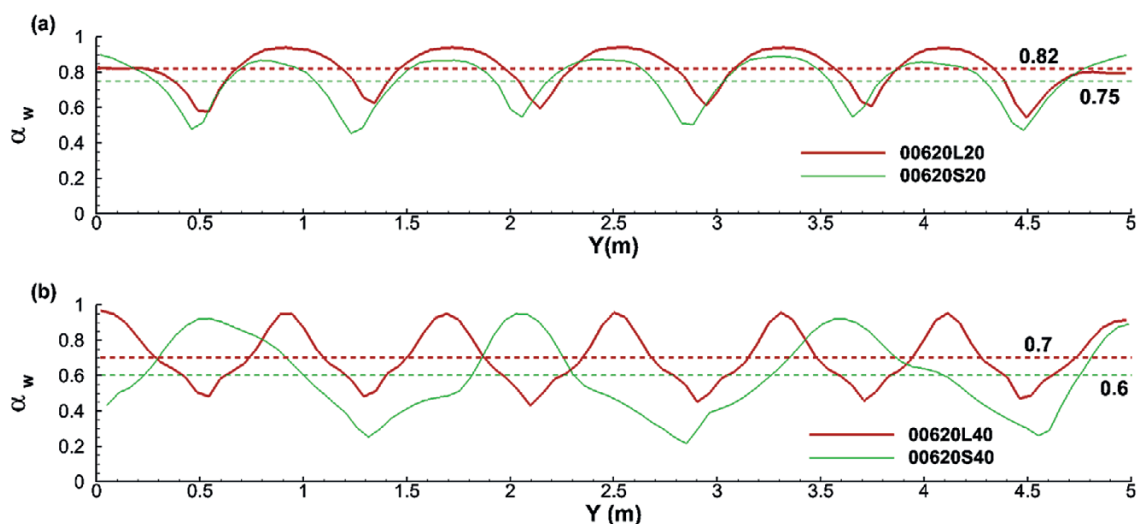


Figure 14

The α_w values across the width of the chute 5 m downstream of x_i for simulations with unit discharge of $20 \text{ m}^3 \cdot \text{s}^{-1} \cdot \text{m}^{-1}$ aerated using (a) 20 cm-diameter aerators, and (b) 40 cm-diameter aerators. Dashed lines indicate the average value of α_w over the span

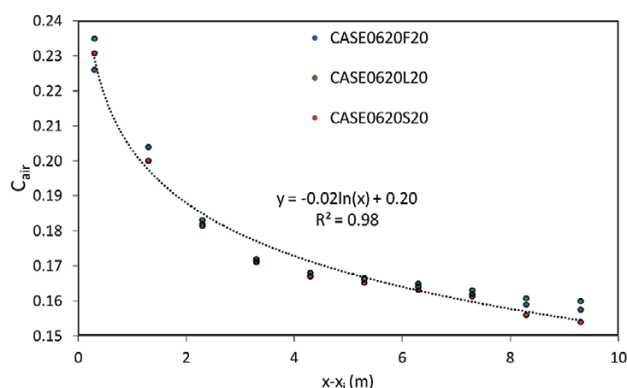


Figure 15

Cross-sectional average air concentration C_{air} calculated at several vertical planes in the streamwise direction after the re-attachment point x_i

SUMMARY AND CONCLUSIONS

The aeration of the flow over a single step on a single slope spillway was studied using 3-dimensional numerical simulations of mid to high discharged supercritical flows. The variables considered in the study are discharge, aerator size, aerator arrangement, Froude number of the flow, presence of a ramp before the step and its angle. The effects of aerators could be evaluated via numerical models with ease while eliminating the scaling factors in physical experiments, which could cause systematic underestimation of the air-entrainment rate and the air-water interfacial properties (Pfister and Chanson, 2014). The concomitant use of physical experiments and the numerical simulations could further the understanding of air-entrainment in spillway flows.

In the present study, L, S and F arrangement of the aerators was observed to affect the jet-length, β , and the degree of lateral uniformity of aeration and total length of aerated regions downstream of the aerators. The conclusions of the present study are:

- S arrangement of aerators is found to be slightly more efficient in terms of increasing the jet-length compared to L and F arrangements at the flow discharge of $20 \text{ m}^3 \cdot \text{s}^{-1} \cdot \text{m}^{-1}$.
- The value of β , hence the air-entrainment, is slightly higher in simulations where aerators are positioned in L arrangement compared to S arrangement.
- The S arrangement of 40 cm-diameter aerators causes merging of air plumes downstream of the re-attachment point. The air concentration, lateral uniformity of aeration and total length of aerated regions near the channel floor increase due to merging, compared to the L arrangement of 40 cm-diameter aerators. Hence, to achieve uniform aeration near channel floor S arrangement of aerators might be a desirable design feature.
- Keeping the total aeration area constant, increasing the aerator size while decreasing the number of aerators, increases the jet-length of the flow; however, it decreases the β index.
- The upward motion of air in the flow after x_i is due to the difference between the specific gravity of water and air, which results in a decrease of C_{air} over the streamwise direction in the de-aeration zone. This decrease is found to be a logarithmic decay in the de-aeration zone.

In the present work, simple k- ϵ model is used for the turbulent flow calculations. The shortcoming of k- ϵ model is that it calculates turbulent diffusion using a single turbulent length scale. In order to observe the turbulence-related features of the flow, advanced turbulence models could be used in the future. The air-entrainment at the free surface of the flow is neglected to better concentrate on the lower nappe air-entrainment; more realistic results are possible if free surface air infusion is also considered. Much wider conclusions on effect of aerator size and arrangement are possible by considering a wider study range for these variables.

REFERENCES

- ANSYS (2011) Fluent 14.0 Theory Guide. ANSYS Inc., Canonsburg, PA. 24 98 pp.
- ARANTES EJ, PORTO RM, GULLIVER JS, LIMA ACM and SCHULZ HE (2010) Lower nappe aeration in smooth channels: experimental data and numerical simulation. *Ann. Braz. Acad. Sci.* **82** (2) 521–537.
- AYDIN MC (2005) CFD analyses of bottom-inlet spillway aerators. PhD Thesis, Graduate School of Natural and Applied Sciences of Elazig University, Elazig.
- AYDIN MC and OZTURK M (2009) Verification and validation of a computational fluid dynamics (CFD) model for air-entrainment at spillway aerators. *Can. J. Civ. Eng.* **36** 826–836. <https://doi.org/10.1139/L09-017>
- BOMBARDELLI FA, MEIRELES I and MATOS J (2011) Laboratory measurements and multi-block numerical simulations of the mean flow and turbulence in the non-aerated skimming flow region of steep stepped spillways. *Environ. Fluid Mech.* **11** 263–288. <https://doi.org/10.1007/s10652-010-9188-6>
- CASSIDY JJ and ELDER RA (1984) Spillways of high dams. In: Novak P (ed) *Developments in Hydraulic Engineering-2*. Elsevier Applied Science Publishers Ltd., Essex, England. 159–182.
- CHANSON H (1990) Study of air demand on spillway aerator. *J. Fluids Eng.* **112** (3) 343–350. <https://doi.org/10.1115/1.2909410>
- COLEMAN HW, SIMPSON AR and DE GARCIA LM (1983) Aeration for cavitation protection of Uribante Spillway. In: *Proceedings of the Conference on Frontiers in Hydraulic Engineering - American Society of Civil Engineers*, 9–12 August 1983, Cambridge, MA, USA. 438–443.
- DEMIROZ E (1985) Spillway aerator project criterions used for high-speed chute flows. TUBITAK, Engineering Research Group, Project 606, Ankara, Turkey.
- HAMILTON WS (1984) Preventing cavitation damage to hydraulic structures: Part 3, Water. *Power Dam Construct.* **36** (1) 42–45.
- KELLS JA and SMITH CD (1991) Reduction of cavitation in spillways by induced air-entrainment. *Can. J. Civ. Eng.* **18** (3) 358–377. <https://doi.org/10.1139/l91-047>
- KOKPINAR MA and GOGUS M (2002) High-speed jet flows over spillway aerators. *Can. J. Civ. Eng.* **29** 885–898. <https://doi.org/10.1139/l02-088>
- KRAMER K (2004) Development of aerated chute flow. PhD thesis, Swiss Federal Institute of Technology Zurich, ETH Zurich.
- LEE W and HOOPES JA (1996) Prediction of cavitation damage for spillways. *J. Hydraul. Eng.* **122** (9) 481–488. [https://doi.org/10.1061/\(ASCE\)0733-9429\(1996\)122:9\(481\)](https://doi.org/10.1061/(ASCE)0733-9429(1996)122:9(481))
- LESLEIGHTER EJ and CHANG HT (1981) Experience on flow aeration to prevent cavitation erosion in spillway chutes. In: *Conference on Hydraulics in Civil Engineering 1981: Preprints of Papers*. Institution of Engineers, Australia. 128.
- OSKOLKOV AG and SEMENKOV VM (1979) Experience in designing and maintenance of spillway structures on large rivers in the USSR. In: *Thirteenth International Congress on Large Dams* **50** 789–802. New Delhi, India.
- PAN S, SHAO Y, SHI Q and DONG X (1980) The self-aeration capacity of the water jet over the aeration ramp. *J. Hydraul. Eng. Beijing, PRC* **5** 13–22. (USBR Translations, Denver, Colorado, USA, February 1983)

- PFISTER M and CHANSON H (2014) Two-phase air-water flows: Scale effects in physical modelling. *J. Hydrodyn.* **26** (2) 291–298. [https://doi.org/10.1016/S1001-6058\(14\)60032-9](https://doi.org/10.1016/S1001-6058(14)60032-9)
- PINTO NLS (1988) Cavitation and aeration. In: Jansen RB (ed) *Advanced Dam Engineering for Design, Construction and Rehabilitation*. Kluwer Academic Publishers, Dordrecht, The Netherlands. 620–634.
- PINTO NLS and NEIDERT SH (1983) Evaluating entrained air flow through aerators. *Water Power Dam Construct.* **35** (8) 40–42.
- PINTO NLS, NEIDERT S and OTA JJ (1982) Aeration at high velocity flows. *Water Power Dam Construct.* **34** (2) 34–38.
- RUTSCHMANN P and HAGER WH (1990) Air-entrainment by spillway aerators. *ASCE J. Hydraul. Eng.* **116** (6) 765–782. [https://doi.org/10.1061/\(ASCE\)0733-9429\(1990\)116:6\(765\)](https://doi.org/10.1061/(ASCE)0733-9429(1990)116:6(765))
- SCHWARTZ I and NUTT LP (1963) Projected nappes subjected to transverse pressure. *ASCE J. Hydraul. Div.* **89** (7) 97–104.
- SINHA SK, SOTIROPOULOS F and ODGAARD AJ (1998) Three-dimensional numerical model for flow through natural rivers. *J. Hydraul. Eng.* **124** (1) 13–25. [https://doi.org/10.1061/\(ASCE\)0733-9429\(1998\)124:1\(13\)](https://doi.org/10.1061/(ASCE)0733-9429(1998)124:1(13))
- TAN P (1984) Model studies of aerators on spillways. Research Report 85-6, Department of Civil Engineering, University of Canterbury, Christchurch, New Zealand.
- TERRIER SCO (2016) Hydraulic performance of stepped spillway aerators and related downstream flow features. PhD thesis, Ecole Polytechnique Federale De Lausanne.
- VOLKART P and RUTSCHMANN P (1991) Aerators on spillways. In: WOOD IR (ed) *Air-Entrainment in Free-Surface Flows: IAHR Hydraulic Structures Design Manual 4*. CRC Press, Rotterdam, The Netherlands. 85–113.
- WEI C and DEFAZIO F (1982) Simulation of free jet trajectories for the design of aeration devices on hydraulic structures. *Proceedings of 4th International Conference on Finite Elements in Water Resources*, June 1982. IAHR, ISCME, DFG, Hanover, Germany.
- ZARRATI AR (1994) Mathematical modelling of air-water mixtures in open channels. *J. Hydraul. Res.* **32** (5) 707–720. <https://doi.org/10.1080/00221689409498710>
-